# Manipulation of pure spin current in ferromagnetic metals independent of magnetization

Dai Tian, Yufan Li, D. Qu, S. Y. Huang, Xiaofeng Jin, and C. L. Chien

Phys. Rev. B **94**, 020403 — Published 5 July 2016

DOI: 10.1103/PhysRevB.94.020403

# Pure Spin Current in Ferromagnetic Metals: Independence of Magnetization

Dai Tian,[1,2] Yufan Li,[2] D. Qu,[2] S.Y.Huang,[3] Xiaofeng Jin,[1] and C. L. Chien[2,*]

[1]*State Key Laboratory of Surface Physics and Department of Physics, Fudan University, Shanghai 200433,China*
[2]*Department of Physics and Astronomy, Johns Hopkins University, Baltimore, Maryland 21218, USA*
[3]*Department of Physics, National Taiwan University, Taipei, 10617, Taiwan*

(Dated: April 28, 2016)

Upon the injection of a pure spin current, a ferromagnet, similar to a non-magnetic metal, also exhibits inverse spin Hall effect (ISHE). We show in Co/Cu/YIG, where the thin Cu layer allows transmission of spin current from YIG into Co but decouples the two ferromagnets, such that the interaction between ISHE and ferromagnetic ordering in Co can be unambiguously investigated. By switching on and off the pure spin current contribution, we demonstrate that the ISHE in Co is independent of the direction of the Co magnetization, which clearly suggest the ISHE in Co is dominated not by the extrinsic impurity scatterings, but from the intrinsic origin.

Spintronics has advanced from the manipulation of spin-polarized current to that of pure spin current. A pure spin current cannot be generated by the usual electrical means except through a few new mechanisms, among them, the spin Hall effect (SHE) [1–3], nonlocal spin valves [4–6], spin pumping [7–9] and the longitudinal spin Seebeck effect (SSE) [10–12]. Particular attractive is the longitudinal SSE [shown schematically in Fig.1 (a)], which generates a spin current by a thermal gradient applied across an insulating ferromagnetic material, without resorting to advanced lithography, high frequency spin excitations, complex measuring schemes, or high current density. The pure spin current injected into an adjacent metal with strong spin orbit coupling is most often detected by the inverse spin Hall effect (ISHE), which converts the spin current $j_s$ into a charge current $j_c$. 5d non-magnetic metals, such as Pt and Au, with strong spin-orbit coupling are common spin current detector materials. The prowess of the spin current detection is measured by the large spin Hall angle $\theta_{SH} = (2e/\hbar)(j_s/j_c)$, where $e$ the electronic charge and $\hbar$ the reduced Planck constant.

Recently, it has been demonstrated that, in addition to non-magnetic metals, ISHE also exists when a pure spin current enters a ferromagnetic (FM) metal. Remarkably, the value of $\theta_{SH}$ in FM permalloy ($Ni_{79}Fe_{21}$) is within 40% of that of Pt, the material with the largest $\theta_{SH}$ [13]. The ISHE in a FM metal also allows the exploration of the interaction of a spin current with magnetization of aligned magnetic moments. One recalls the giant magnetoresistance (GMR) effect [14, 15] and the spin transfer torque effect in multilayers of FM metals [16, 17]. At sufficiently high current density, both a spin-polarized current and a pure spin current can induce switching of magnetization or domain wall motion [18–21]. However, the counterpart effect, the influence of the magnetization on the ISHE in a ferromagnetic metal has never been addressed. In fact, the structure of Py/YIG, where ISHE in FM materials was first demonstrated [13], precludes such investigations because Py and YIG are so strongly coupled that their magnetization directions are locked. In addition, under a vertical temperature gradient, the FM metal also generates the anomalous Nernst effect (ANE), schematically shown in Fig. 1(b), that entangles with the longitudinal SSE in Py/YIG.

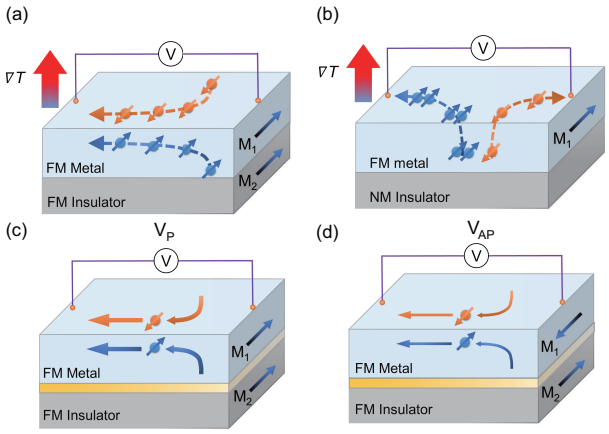


FIG. 1: Schematics of (a) longitudinal spin Seebeck effect induced inverse spin Hall effect (b) anomalous Nernst effect in a ferromagnetic metal, both under a vertical temperature gradient. It illustrates the generation of a charge current from a spin current in SSE in (a), and a spin polarized current due in ANE in (b), where $M_1$ and $M_2$ are the magnetization of the two FM layers. (c)(d) present the injected spin current under parallel configuration and anti-parallel configuration when $M_1$ and $M_2$ are magnetically decoupled by a intervening non-magnetic layer(yellow).

In this work, we designed a special Co/Cu/YIG structure, in which the thin intervening Cu layer magnetically decouples FM metal Co and FM insulator YIG but allowing the transmission of pure spin current [22]. The spin index of the pure spin current is set by the direction of the YIG magnetization $M_{YIG}$, whereas the Co magnetization $M_{Co}$ direction can be arbitrarily and independently controlled, such as those shown in Fig. 1(c) and (d) with parallel and antiparallel magnetizations. We show that the ISHE remains the same for *any* orientation of $M_{Co}$ relative to $M_{YIG}$. It is therefore evident that the ISHE in Co is not dominated by impurity-scattering related

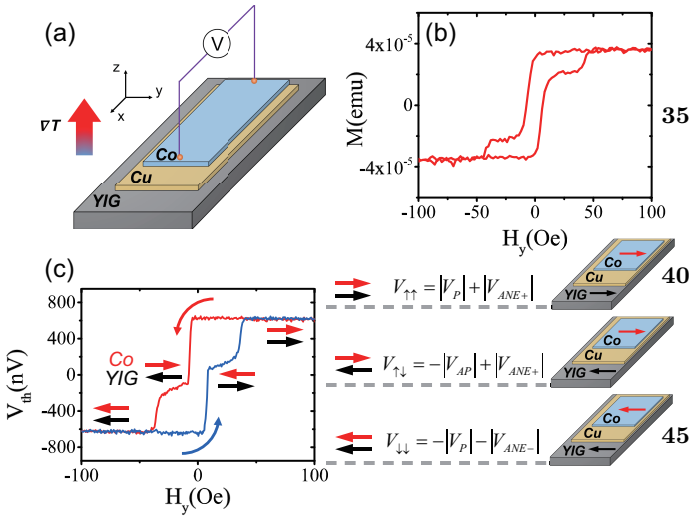


FIG. 2: (a) Multilayer Co/Cu/YIG structure with the thermal gradient in the z-direction. (b) Magnetization switching of Co(2 nm)/Cu(5 nm)/YIG(120 nm). (c) Thermal voltage measurement of Co(3.5 nm)/Cu(5 nm)/YIG(120 nm), where field decreasing and field increasing branches are denoted as red and blue. The configurations of three magnetization steps and voltages are shown in the right.

mechanisms, but an intrinsic property resulted from the band structure.

We used RF magnetron sputtering to deposit YIG (yttrium iron garnet = $Y_3Fe_5O_{12}$) films with thickness of about 120 nm on GGG (gadolinium gallium garnet) (111) single crystal substrates. The as-deposited YIG films are not magnetic but become ferrimagnetic after annealing at 850°C for 4 hours in flowing $O_2$. We then deposited onto the YIG thin film at room temperature a thin Cu layer of 5nm followed by a Co layer of several thicknesses to achieve the trilayer structure as illustrated in Fig. 2(a). Each sample was spin-coated with photoresist immediately after taken out of the vacuum. The insertion of the Cu(5nm) layer is to magnetically decouple Co and YIG but allowing the transmission of the spin current injected from YIG into Co. As an example, the hysteresis loop of Co(2 nm)/Cu(5 nm)/YIG(120 nm) with an in-plane magnetic field measured by a vibrating sample magnetometer (VSM) is showed in Fig. 2(b). The two independent switchings of magnetizations originate from the different coerivities ($H_c$) of YIG and Co of 5 Oe and 50 Oe, respectively. This confirms that with the insertion of Cu layer, the YIG and the Co layers are decoupled and switch at very different magnetic fields.

We use the longitudinal SSE by subjecting the structure to a temperature gradient near room temperature along the out-of-plane z directions as shown in Fig. 2(a), injecting the spin current $j_s$ from YIG into Co across the Cu layer. The spin index $\hat{\sigma}$ is set by $M_{YIG}$ and points to the +y direction under an appropriate positive magnetic field. When $j_s$ enters the Co layer, an electric field rises as the result of the ISHE, $E_{SSE} \propto \vec{j}_s \times \hat{\sigma}$, detected as an ISHE voltage. Therefore, the polarity of the ISHE voltage is set by the $M_{YIG}$.

However, since Co is a FM metal, in additional to the ISHE voltage, the thermal gradient also induces the anomalous Nernst effet(ANE) of $E_{ANE} \propto \nabla T \times \vec{M}_{Co}$, thus additional efforts are required to separate out the contributions from ANE and SSE. The decoupling of the Co and YIG layers allow us to control $M_{YIG}$ and $M_{Co}$ independently to separate the two effects.

We have patterned the multilayer into a Hall bar structure where all the segments are 0.5 mm in width and the separation between two adjacent probe is 3 mm. Referring to Fig. 2(a), the Hall-bar is situated along the x direction, the thermal gradient $|\nabla T|$ of about 40 K/mm is along the z-axis, the magnetic field H is along the y direction. More details of the experimental setup can be found in the Supplemental Material[23]. The thermal voltage of $V_{th}$ vs. $H_y$ obtained from Co(3.5 nm)/Cu(5 nm)/YIG(120 nm) is shown in Fig. 2(c). Since the YIG and Co switch independently at different fields, there are several distinct voltages that can be clearly associated with the particular configurations of magnetization direction as revealed in Fig. 2(c). First, at a large positive field, $M_{YIG}$ and $M_{Co}$ are aligned in the +y direction, thus the $V_{th} = |V_P| + |V_{ANE+}|$, where the $V_P$ denotes the voltage arises from the ISHE when $M_{YIG}$ and $M_{Co}$ are parallel to each other, and $V_{ANE}$ denotes the voltage from the ANE in Co. When the $M_{YIG}$ is switched to the −y direction at a field of about −5 Oe, $M_{Co}$ remains in +y, the polarity of the SSE switches from positive to negative while ANE remains as positive, therefore the $V_{th} = -|V_{AP}| + |V_{ANE+}|$. The $V_{AP}$ denotes the voltage arising from the ISHE when $M_{YIG}$ and $M_{Co}$ are antiparallel. As the magnetic field is changed to around −40 Oe (slightly smaller than the $H_c$ of 2 nm Co), $M_{Co}$ switches to −y, thus $V_{th} = -|V_P| - |V_{ANE-}|$, which is symmetric with that of the positive field. In general, $|V_{ANE-}| = |V_{ANE+}|$, but $|V_P|$ may be different from $|V_{AP}|$.

To extract $|V_P|$ and $|V_{AP}|$, one needs to determine the value of $|V_{ANE-}|$ or $|V_{ANE+}|$. This can be accomplished by exploiting ways to suppress one of the two effects, such as the spin current contribution. For example, the spin current can be blocked by replacing YIG with a nonmagnetic material, or modifying the interface of YIG using Ar-ion bombardment or inserting a barrier layer (MgO) [13]. These methods require two different samples, one generates only ANE and the other generates both SSE and ANE. However, with two samples, it is difficult to assure ANE to be the same in both cases.

We use instead one single Co/Cu/YIG sample and exploit the difference in the coercivities of Co and YIG and the angular dependency. We demonstrate that the SSE contribution in our measurement can be reversibly switched on and off. The thermal voltage for both ANE

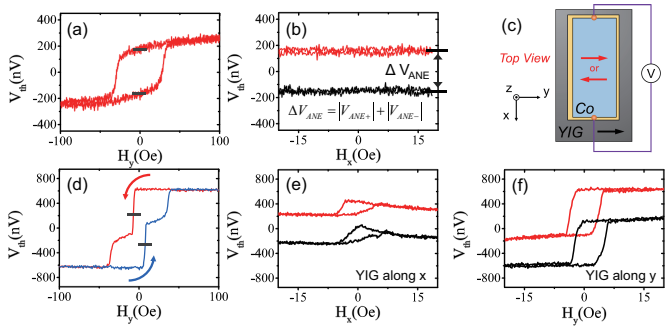


FIG. 3: ANE voltages obtained from Co/Cu/Si, with (a) large magnetic field along y direction and (b) small field along x direction. Thermal voltage obtained from Co/Cu/YIG under the scheme shown in (c), with (d) a large magnetic field along y direction and (e) a small field along x direction after Co magnetization has been set along the +y (red) and −y (black) direction. (f) Small field along y after Co magnetization has been set along +y (red) and −y (black) direction. The loop height measures $\Delta V_{SSE}$, and centroid gives $V_{ANE}$.

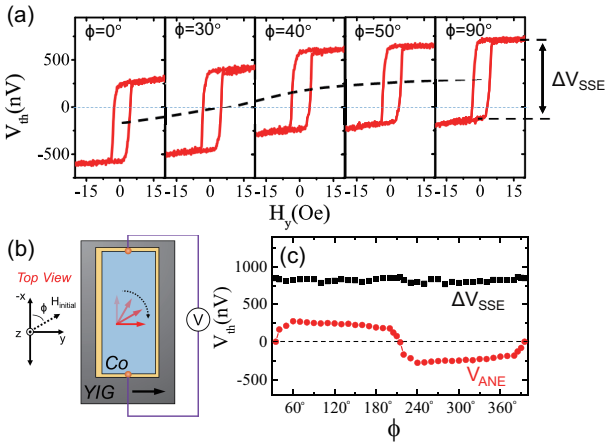


FIG. 4: (a) Thermal voltage $V_{th}$ versus $H_y$ while a small field is swept along the y-axis, after Co magnetization has been set by a large field $H_{initial}$ along the $\phi$ direction with respect to the x-axis. The experimental setup is shown in (b). (c) The full angular dependence of $\Delta V_{SSE}$ and $V_{ANE}$.

and SSE have the same angular dependence as showed in Fig. 2(c), both $V_{ANE}$ and $V_{SSE}$ reach the maximum absolute value when $M_{Co}$ and $M_{YIG}$ are along the y direction, and drop to zero when along the x direction. Since the coecivity of Co is larger than that of YIG, we first use $H_y = 150$ Oe to align both $M_{Co}$ and $M_{YIG}$ to the y direction. After that, we decrease $H_y$ to 0 Oe, and scan $H_x$ from 20 Oe to −20 Oe. In this small field range of ±20 Oe, $H_x$ switches YIG but not Co because of its larger $H_c$. As a result, $V_{ANE}$ to remain unchanged while $V_{SSE} = 0$.

To check the viability of this method, we first apply it to the Co(3.5 nm)/Cu(5 nm)/Si structure, which exhibits only ANE. Under $H_y$ one observes the loop due to ANE as shown in Fig. 3(a). After returning to $H_y = 0$ Oe and under $H_x$ of ±20 Oe, one observes constant $V_{ANE+}$ (red) and $V_{ANE-}$ (black) within the field range (as shown in Fig. 3(b)) indicating that $M_{Co}$ remains set at +y and −y direction as intended. The two values of $V_{ANE}$ obtained are consistent, indicating that a very small $H_x$ does not significantly affect the direction of $M_{Co}$.

We then apply the method to Co/Cu/YIG as schematically shown in Fig. 3(c). The full switching results with a large $H_y$ range is shown in Fig. 3(d), which is similar to Fig. 2(c). We then align $M_{YIG}$ and $M_{Co}$ to the +y (or −y) direction, and scan $H_x$ in ±20 Oe as shown as red (or black) curve in Fig. 3(e). The small loops around 5 Oe is due to the switching and rotation of $M_{YIG}$. The difference of the black and the red curves gives the value of the $\Delta V_{ANE} = |V_{ANE+}| + |V_{ANE-}|$= 501±24 nV. The two short black lines in Fig. 3(d) denote $V_{ANE+}$ and $V_{ANE-}$ obtained from Fig. 3(e). Given that $V_{th} = |V_P| + |V_{ANE+}|$ at $H_y = 150$ Oe and $V_{th} = -|V_{AP}| + |V_{ANE+}|$ at $-12$ Oe $< H_y < -8$ Oe, we obtain $|V_P| = 375\pm27$ nV and $|V_{AP}| = 361\pm19$ nV. Similar result has also been observed for 5 nm thick Co.

We then apply a large field along the +y direction (−y direction) to align $M_{YIG}$ and $M_{Co}$, return to zero field, scan $H_y$ in the ±20 Oe range, one observes only the red (black) SSE loop as illustrated in Fig. 3(f). It is important to note the height of the loop gives $\Delta V_{SSE}$, the magnitude of the SSE, the centroid of the loop gives the value of $V_{ANE}$, which is positive (negative) for the red (black) loop. In this manner, the SSE and ANE can be completely separated. From Fig. 3(f), it is clear that for P and AP arrangements, $\Delta V_{SSE}$ remains the same. Because of the sinusoidal angular dependence of SSE, one needs measurements other than P and AP.

Now we apply this method to any angle $\phi$ with respect to the x-axis by first applying a large field $H_{initial}$ along the $\phi$ direction and then perform measurements with $H_y$ in the ±20 Oe, as schematically shown in Fig. 4(b). Some examples with $\phi = 0°$, 30°, 40°, 50°, and 90° are shown in Fig. 4(a). It is immediately clear that in each case the loop height, which measures $\Delta V_{SSE}$, remains unchanged, while the centroid of the loop, which measures $V_{ANE}$, changes with $\phi$. The full angular dependence of $\Delta V_{SSE}$ and $V_{ANE}$ are shown in Fig. 4(c). The value of $\Delta V_{SSE}$ is independent of $\phi$, the set angle between $M_{Co}$ and $-x$ axis, in other words, the angle between spin index of the pure spin current and $M_{Co}$. The ISHE in a FM metal is *independent* of its magnetization.

In our measuring scheme, we first align the $M_{Co}$ in the $\phi$ direction with a large field $H_{initial}$. When the large field $H_{initial}$ is switched off, the $M_{Co}$ returns to its remnant magnetization, most often without the full $|M_{Co}|$ in the ideal $\phi$ direction due to magnetic anisotropy of the rectangularly shaped Co layer. Thus $V_{ANE}$ is clearly periodic with a period of $2\pi$, but $V_{ANE}$ does not display the

simple angular dependence of $\sin(\phi)$ with $V_{ANE} = 0$ nV at $\phi = 0°$ but instead at about 35°. However, since the $\Delta V_{SSE}$ is constant regardless of $M_{Co}$, it is certainly independent of the remnant magnetization of Co, whatever its value.

We now discuss our experimental findings in the light of the underlying mechanisms of the SHE; the implication of the observed M independence will hence become clear. It is widely accepted that the SHE and the anomalous Hall effect (AHE) share the same origin [24, 25], of which three mechanisms has been proposed to account for the left-right asymmetry. Among them, the skew scattering [26] and the side jump [27] are related to impurity scatterings, known as the extrinsic mechanisms; and the intrinsic mechanism, which is solely determined by the electronic band structure, results spin-up and spin-down carriers to gain opposite transverse velocity when driven by an electrical field [28, 29]. The AHE resulted by the extrinsic mechanisms must come from at least one of the three scenarios depicted in Fig. 5; those are, (i) a spin-polarized current being scattered by a non-magnetic impurity [Fig. 5(a)] or (ii) a magnetic impurity [Fig. 5(b)], and (iii) a non-polarized current being scattered by a magnetic impurity, as shown in Fig. 5(c). Scenario (i) and (ii) have been evidenced by ample experiments involving various dopants in ferromagnetic metals [30, 31]. Scenario (iii) is evidenced by the AHE observed in paramagnetic materials [32–34]. It then becomes obvious that the Hall angle resulted by (i) and (ii) must be different, otherwise (iii) cannot produce observable AHE, for spin-up and spin-down electrons will gain opposite transverse velocity that cancels the transverse charge accumulation. Therefore, the SHE originated from the extrinsic mechanisms must depend on the magnetization, which contradicts to our observation[35]. Our findings thus unambiguously exclude the extrinsic mechanisms as the dominating mechanism for the ISHE observed in Co, and instead point to the intrinsic origin. This is consistent with observations of AHE in Co thin films, which appears to be also dominated by the intrinsic contribution [36].

In summary, using Co/Cu/YIG, where Cu decouples the ferromagnetic Co and YIG but allowing transmission of pure spin current, we have separately observed SSE and ANE, and show that the ISHE in a FM metal is *independent* of its magnetization. It therefore provides an unambiguous evidence that the ISHE in Co is dominated not by the extrinsic impurity-scattering mechanisms, but the intrinsic one.

This work was supported as part of SHINES, an EFRC center funded by the U. S. Department of Energy, Office of Science, Basic Energy Science, under award SC0012670. D.Q. was supported by STARnet, a SRCprogram sponsored by MARCO and DARPA.

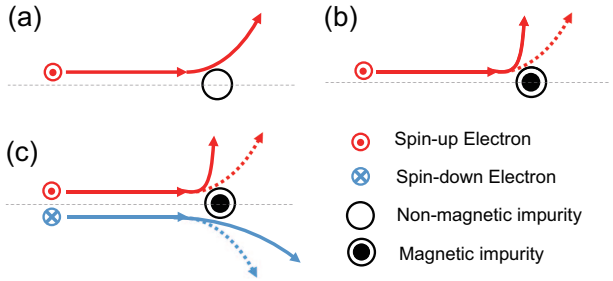


FIG. 5: Schematic drawing of three scenarios of extrinsic AHE, (a) polarized current scattered by non-magnetic impurity; (b) polarized current scattered by magnetic impurity; and (c) non-polarized current scattered by magnetic impurity. The dashed lines indicate trajectories of the carriers if the impurity were non-magnetic.

* Electronic address: clchien@jhu.edu

[1] M. I. Dyakonov and V. I. Perel, Phys. Lett. **35**, 459 (1971).
[2] Y. Kato, R. Myers, A. Gossard, and D. Awschalom, science **306**, 1910 (2004).
[3] J. E. Hirsch, Phys. Rev. Lett. **83**, 1834 (1999).
[4] S. O. Valenzuela and M. Tinkham, Nature **442**, 176 (2006).
[5] T. Kimura, Y. Otani, T. Sato, S. Takahashi, and S. Maekawa, Phys. Rev. Lett. **98**, 156601 (2007).
[6] T. Seki, Y. Hasegawa, S. Mitani, S. Takahashi, H. Imamura, S. Maekawa, J. Nitta, and K. Takanashi, Nature Materials **7**, 125 (2008).
[7] E. Saitoh, M. Ueda, H. Miyajima, and G. Tatara, Appl. Phys. Lett **88**, 182509 (2006).
[8] K. Ando, Y. Kajiwara, S. Takahashi, S. Maekawa, K. Takemoto, M. Takatsu, and E. Saitoh, Phys. Rev. B **78**, 014413 (2008).
[9] O. Mosendz, J. E. Pearson, F. Y. Fradin, G. E. W. Bauer, S. D. Bader, and A. Hoffmann, Phys. Rev. Lett. **104**, 046601 (2010).
[10] S. Y. Huang, W. G. Wang, S. F. Lee, J. Kwo, and C. L. Chien, Phys. Rev. Lett. **107**, 216604 (2011).
[11] D. Qu, S. Y. Huang, J. Hu, R. Wu, and C. L. Chien, Phys. Rev. Lett. **110**, 067206 (2013).
[12] T. Kikkawa, K. Uchida, Y. Shiomi, Z. Qiu, D. Hou, D. Tian, H. Nakayama, X.-F. Jin, and E. Saitoh, Phys. Rev. Lett. **110**, 067207 (2013).
[13] B. F. Miao, S. Y. Huang, D. Qu, and C. L. Chien, Phys. Rev. Lett. **111**, 066602 (2013).
[14] M. N. Baibich, J. M. Broto, A. Fert, F. N. Van Dau, F. Petroff, P. Etienne, G. Creuzet, A. Friederich, and J. Chazelas, Phys. Rev. Lett. **61**, 2472 (1988).
[15] G. Binasch, P. Grünberg, F. Saurenbach, and W. Zinn, Phys. Rev. B **39**, 4828 (1989).
[16] J. C. Sankey, Y.-T. Cui, J. Z. Sun, J. C. Slonczewski, R. A. Buhrman, and D. C. Ralph, Nature Physics **4**, 67 (2008).
[17] L. Liu, T. Moriyama, D. C. Ralph, and R. A. Buhrman, Phys. Rev. Lett. **106**, 036601 (2011).
[18] L. Liu, C.-F. Pai, Y. Li, H. Tseng, D. Ralph, and

R. Buhrman, Science **336**, 555 (2012).
[19] T. Yang, T. Kimura, and Y. Otani, Nature Physics **4**, 851 (2008).
[20] A. Yamaguchi, T. Ono, S. Nasu, K. Miyake, K. Mibu, and T. Shinjo, Phys. Rev. Lett. **92**, 077205 (2004).
[21] L. Thomas, M. Hayashi, X. Jiang, R. Moriya, C. Rettner, and S. S. Parkin, Nature **443**, 197 (2006).
[22] D. Tian, Y. Li, D. Qu, X. Jin, and C. L. Chien, Appl. Phys. Lett **106**, 212407 (2015).
[23] See Supplemental Material at [URL will be inserted by publisher] for more experimental setup details.
[24] N. Nagaosa, J. Sinova, S. Onoda, A. H. MacDonald, and N. P. Ong, Rev. Mod. Phys. **82**, 1539 (2010).
[25] A. Hoffmann, IEEE transactions on magnetics **49**, 5172 (2013).
[26] J. Smit, Physica **24**, 39 (1958), ISSN 0031-8914.
[27] L. Berger, Phys. Rev. B **2**, 4559 (1970).
[28] R. Karplus and J. M. Luttinger, Phys. Rev. **95**, 1154 (1954).
[29] G. Sundaram and Q. Niu, Phys. Rev. B **59**, 14915 (1999).
[30] A. K. Majumdar and L. Berger, Phys. Rev. B **7**, 4203 (1973).
[31] Y. Shiomi, Y. Onose, and Y. Tokura, Phys. Rev. B **79**, 100404 (2009).
[32] A. Fert and O. Jaoul, Phys. Rev. Lett. **28**, 303 (1972).
[33] A. Fert, A. Friederich, and A. Hamzic, Journal of Magnetism and Magnetic Materials **24**, 231 (1981), ISSN 0304-8853.
[34] Y. Li, D. Hou, L. Ye, Y. Tian, J. Xu, G. Su, and X. Jin, EPL (Europhysics Letters) **110**, 27002 (2015).
[35] The extrinsic scattering consists of scattering by non-magnetic impurities, and magnetic impurities, and the latter includes defects in Co itself. While one cannot quantify the various contributions to the transport properties, in the present case of polycrystalline Co the contribution from crystalline defects dominates.
[36] D. Hou, Y. Li, D. Wei, D. Tian, L. Wu, and X. Jin, Journal of physics. Condensed matter : an Institute of Physics journal **24**, 482001 (2012), ISSN 0953-8984.